NUCLEOSIDES & NUCLEOTIDES, 18(11&12), 2785-2818 (1999)

The Physico-chemical Properties of 5'-Polyarene Tethered DNA-Conjugates, and their Duplexes with Complementary RNA

Nitin Puri and Jyoti Chattopadhyaya*

Department of Bioorganic Chemistry, Box 581, Biomedical Center, University of Uppsala, S-751 23 Uppsala, Sweden

E-mail: jyoti@bioorgchem.uu.se. Fax: +4618-554495

ABSTRACT: Fluorophores **1**-**13** when covalently linked to the 5'-terminus of 9-mer ssDNA (as in ssDNA-conjugates **16**-**28**) enhance the stablity of the duplexes with both RNA (**29**) and DNA (**30**) targets compared to the natural counterparts, which, for the first time, demonstrated the effect of the bulk and the π-electron density of various 5'-tethered fluorophores on the heteroduplex stability. It has been found that decreasing the π-electron density of the fluorophore induces a more favourable π-π interaction with the adjacent nucleobase, leading to higher duplex stability. Increasing the surface-area of 5'-stacked fluorophore only increases the thermal stability of the duplex, if it leads to an increase in the area of π-overlap with the adjacent nucleobase. The fluorescence characteristics show that the tethered-fluorophores stack to the exterior of the terminal nucleobase pair, except for 5'-tethered-α-Napthalene (**10**), which shows dramatic enhancement in fluorescence as normally observed for the minor groove binders. CD data shows that tethering the DNA with different fluorophores at the 5'-end did not make any gross changes in the helical structure of the duplexes of DNA-conjugates with RNA and DNA targets compared to the natural counterparts. It has emerged that the 5'-tethered fluorophores assist in pre-organising the ssDNA-conjugates into a helical conformation more effectively by a stronger fluorophore-nucleobase stacking than in the native ssDNA. All DNA-conjugates tested assisted in cleavage of the complementary RNA strand by RNase H. The RNase H activation by 5'-conjugated DNA-RNA duplex decreased with the decrease of their thermal stabilities, and as they deviated from the structure of the corresponding native DNA-RNA duplex. It has been also found that both native and conjugated DNA-DNA duplexes can indeed block the RNase H activity, thereby reducing the effect of a potential antisense agent. This implies that the palindromic as well hairpin-forming sequences of antisense DNA should be avoided.

INTRODUCTION

Utility of ssDNA with its inherent hydrogen bonding specificity can be enhanced by the covalent linkage to a functionality. These active functionalities can endow ssDNA with improved binding, cell permeability or cleaving characteristics, thereby making them attractive for diagnostic and therapeutic purposes. The first potentially active functionalities were originally developed for specific and irreversible modification of DNA[1] and for augmenting[2] the affinity and specificity of Watson-Crick base pairing of DNA-conjugates towards their complementary targets.

The synthesis and utility of DNA-conjugates tethered with intercalating, cross-linking and alkylating agents has been extensively investigated[3,4] for application in antisense and antigene therapeutics. To facilitate the cellular uptake of natural as well as modified antisense oligos, agents such as cyclodextrins[5], cholesterol[6] and adamantane[5,6c] have been covalently attached to the DNA termini.

Agents[7] like EDTA-Fe(II)[7a], *o*-phenanthroline-Cu(I)[7b]and porphyrin[7c,d] when covalently attached to oligos have brought about specific cleavage of DNA. Oligonucleotide linked with novel photocleavage agents which on excitation cause scission of nucleic acid chain have recently been reviewed[8]. For site-specific cleavage of RNA, agents based on metal complexes, organic catalysts and nuclease enzymes have been coupled to oligonucleotides[9].

Clearly, these 3'- or 5'-DNA-conjugates will find more usefulness, if one can shed light on their structures as well as of their complexes with various targets, and correlate them with their specific function. In this regard, NMR structural studies[10] in solution on *N*-(2-hydroxyethyl)phenazinium (HPznm) linked DNA-DNA[10a] and DNA-RNA duplex[10b] have been reported from our laboratory. These studies showed that the tethered-HPznm enhances the DNA-DNA and DNA-RNA duplex stability by promoting HPznm stacking with the neighbouring nucleobase, leading to reduced rate of exchange of imino protons (particularly of the terminal imino proton adjacent to the tethered fluorophore) with the bulk water as well as by reducing the availability of the first spine of hydration at the core part of the duplex.

Recently, by systematic change of the bulk and π-electron density of the 5'-tethered fluorophores, we were able to demonstrate[11] predictable influence on the thermal stability of the DNA-DNA duplex, but no correlation of the thermal stability with the changes in global helical structure and local geometry of fluorophore binding were attempted.

We have herein elucidated the modes of interaction amongst the π-stackers (*i.e.* the tethered fluorophore and the adjacent nucleobases) that cause either enhancement or reduction of the thermal stability of the conjugated DNA-RNA duplex in comparison with the corresponding DNA-DNA duplex[11]. In this work, we have also attempted to shed light on how the 5'-tethered fluorophore influences the global structure of the resulting duplex, by

examining the CD spectra of the conjugated DNA-RNA and DNA-DNA duplexes, whereas the local geometry of the fluorophore-nucleobase interaction has been elucidated by the fluorescence studies by comparison with earlier reported NMR studies[11]. These CD and fluorescence studies on these tethered duplexes have been finally correlated with their thermodynamic stabilities, giving a molecular insight into how the nature of the 5'-tethered fluorophore actually stabilizes or destabilizes duplexes. It is noteworthy in this context that with the exception of minor groove binder Hoechst 33258[12], very little attempt has been made to explore the molecular mechanism of how a 3'- or 5'-tethered fluorophore actually stabilizes a duplex or a triplex.

It has been also shown (i) that the RNA strand of the heteroduplexes of DNA conjugates **17**, **19**, **21**, **23** and **27** are indeed cleaved by RNase H (the relative rate being dependent on the thermal stability as well as the structure of the hybrid duplex), and (ii) that conjugated DNA-DNA duplexes (**16-28**)•(**30**) can indeed block the RNase H activity, thereby reducing the effect of a potential antisense agent.

RESULT AND DISCUSSION

(A) Synthesis of 5'-fluorophore-tethered 9-mers 16-28 for duplex studies.

Tethering of different agents at the terminus can be achieved by standard solid-phase synthesis[13] or by post-synthetic modification[14], out of which the former was adopted for the synthesis of DNA-conjugates **16-28**. The synthesis of hydroxyalkyl fluorophores **1-7** and **10-13** (FIG. 1) has been reported earlier[11]. Fluorophores 6-{4-[(*N*-(2-hydroxyethyl)-*N*-methyl)aminomethyl]phenyl} phenanthridine (Ptd) **8** and 6-{4-[(*N*-(2-hydroxyethyl)-*N*-methyl)aminomethyl]phenyl}-3,8-dinitrophenanthridine (DnPtd) **9** (FIG. 1) were obtained by condensing 4-(6-phenanthridinyl)-1-benzylchloride and 4-{(3,8-dinitro)-6-phenanthridinyl}-1-benzylchloride respectively with 2-(*N*-methylamino)ethanol in CH_2Cl_2 in the presence of diisopropylethylamine (DIPEA) in 82% yield. The synthesis of 4-(6-phenanthridinyl)-1-benzylchloride and 4-{(3,8-dinitro)-6-phenanthridinyl}-1-benzylchloride was based on published procedures[2a]. Compounds Ptd **8** and DnPtd **9** were converted into corresponding

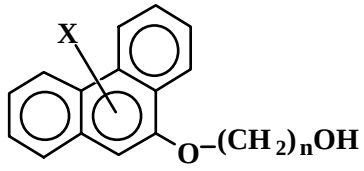

1: X = H, n = 2; (**Phn**)
2: X = NO_2, n = 2; (**NPhn**)
3: X = H, n = 4; (**Phnbu**)

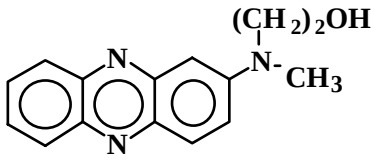

4 (**Pzn**)

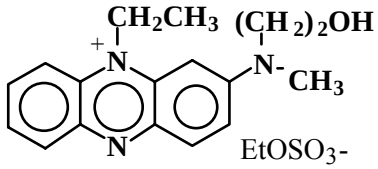

5 (**Pznm**)

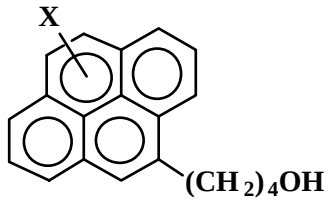

6: X = H; (**Pyr**)
7: X = NO_2; (**NPyr**)

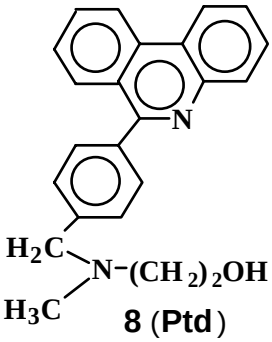

8 (**Ptd**)

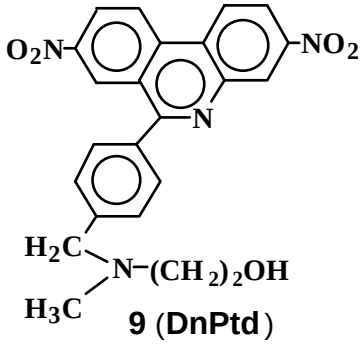

9 (**DnPtd**)

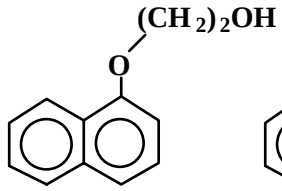

10 (**α-Napth**)

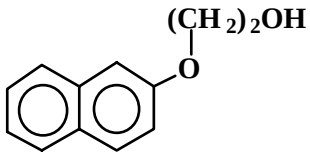

11 (**β-Napth**)

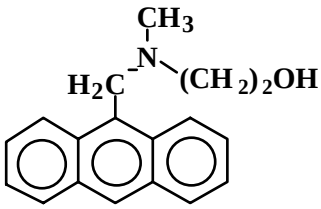

12 (**Anth**)

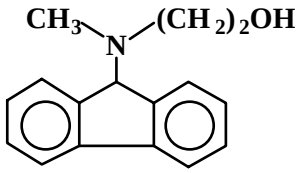

13 (**Flo**)

(A) Non-tethered oligos

14: 3'-d(T A C A A A C C T)-5' (9-mer DNA)

15: 3'-d(U A C A A A C C U)-5' (9-mer RNA)

(B) Nonamer conjugate **16-28**: 3'-d(T A C A A A C C T)-5'-$OP(O_2)^-$-**X**)

(X = corresponding alkoxy moiety of the alcohols **1**-**13**)

16 : X = (**1**)	**19** : X = (**4**)	**22** : X = (**7**)	**25** : X = (**10**)	**28** : X = (**13**)
17 : X = (**2**)	**20** : X = (**5**)	**23** : X = (**8**)	**26** : X = (**11**)	
18 : X = (**3**)	**21** : X = (**6**)	**24** : X = (**9**)	**27** : X = (**12**)	

(C) Single strand targets for duplex formation

29: 5'-d(C A U GU U U G G A)-3' (10-mer RNA)

30: 5'-d(C A T G T T T G G A)-3' (10-mer DNA)

FIG. 1. Polyarenes **1**-**13** tethered to 5'-terminus of 9-mer DNA **14** to give DNA-conjugates **16**-**28**. These DNA-conjugates along with **14** and 9-mer RNA **15** were complexed with 10-mer RNA target **29** and 10-mer DNA target **30**.

amidites[15] and used for solid-phase synthesis[13] of 5'-tethered oligonucleotides **23** and **24**. The synthesis of 5'-fluorophore-tethered oligonucleotides **16-22** and **25-28** from fluorophores **1-7** and **10-13** has been reported earlier[11,16]. Deprotection and purification of oligonucleotides **14-30** (FIG. 1) have been performed using our reported procedure[11].

(B) Thermal stabilities of the duplex formed between 5'-tethered DNA 9-mers 14-28 and RNA target 29.

Duplexes were generated by hybridisation of 5'-tethered 9-mers **14-28** with target RNA **29** in a 1:1 ratio with 1μM concentration of each strand in 20 mM PO_4^{3-}, 0.1 M NaCl buffer at pH 7.3. The temperature range used for the heteroduplex melting study was 10 - 55 ° C. At the starting temperature of 10° C, the baseline of the duplex melting curves showed the duplexes to be at least 98% complexed (details in the experimentals). TABLE 1 shows the melting temperatures (T_m). Following comparisons are noteworthy (ΔT_m indicates increase/decrease of T_m with respect to the native oligo) : (i) With RNA target **29**, all 5'-fluorophore DNA-conjugates enhanced the thermal stability of the heteroduplex (T_m = 21-30° C; ΔT_m = 1-10° C) compared to the non-tethered natural DNA-RNA duplex (T_m = 20° C). (ii) Phenazine (Pzn) tethered DNA-conjugate **19** gave the highest stabilisation of the heteroduplex (T_m = 30° C; ΔT_m = 10° C) amongst all the DNA-RNA duplexes (**16-28**)•(**29**) studied. Replacing anthracene (Anth) ring system in **27** (T_m = 21° C; ΔT_m = 1° C) by Pzn as in **19** (compare entries# 6 & 14 in TABLE 1) leads to a decrease in the π-electron density of the fluorophore which resulted in substantial increase in duplex stabilisation. (iii) Decreasing the π-electron density of the tethered phenanthrene (Phn) (**16•29:** T_m = 26.9° C) to that in nitro-phenanthrene (NPhn) (**17•29:** T_m = 28.2° C), pyrene (Pyr) (**21•29:** T_m = 23.0° C) to that in nitro-pyrene (NPyr) (**22•29:** T_m = 24.6° C) and Ptd (**23•29:** T_m = 25.4° C) to that in DnPtd (**24•29:** T_m = 26.8° C) also showed increase in the duplex stabilisation (compare entries# 3 & 4, 8 & 9 and 10 & 11 in TABLE 1). (iv) For the angular Phn derivatives (compare entries# 3 & 5 in TABLE 1), increasing the linker length as in **16** (T_m = 26.9° C) with two methylenes to that in **18** (T_m = 25.9° C) decreased the duplex stabilisation. (v) Anth-tethered **27** (T_m = 21.1° C) and fluorene (Flo)-tethered **28** (T_m = 21.0° C) gave the lowest duplex stabilisations (ΔT_m = 1° C). Anth-linked **27** (entry# 14 in TABLE 1) showed a lower stabilisation as compared to its angular counterpart Phn-linked **16** (T_m = 26.9° C) (entry# 3 in TABLE 1). (vi) Increasing the surface area as in Pyr-tethered **21** (T_m = 23.0° C) (entry# 8 in TABLE 1) showed a decrease in stabilisation compared to Phnbu-tethered **18** (T_m = 25.9° C) with a linker chain of similar length (entry# 5). (vii) The 9-*N*-ethylphenazinium (Pznm)-linked **20** (T_m = 27.1° C) (entry# 7 in TABLE 1), with a lower π-electron density than Pzn-linked **19** (T_m = 29.9° C), showed lower duplex stabilisation (ΔT_m = 6.8° C). (viii) Of the two naphthalene derivatives, the tethered β-isomer (β-Napth) gave a marginally higher stabilisation (T_m = 23.4° C) than the α-isomer (α-Napth) (T_m = 22.9° C) (compare entries# 12 & 13 in TABLE 1). (ix) The RNA-RNA duplex **15•29** (T_m = 33.3° C) shows much higher stability than the DNA-DNA duplex

14•30 (T_m = 26.2° C) & DNA-RNA duplex **14•29** (T_m = 20.3° C). This is consistent with the comparative values reported[17] for RNA-RNA, DNA-RNA and DNA-DNA duplexes with similar sequence (similar % of pyrimidine bases and fraction of A•T/U base pairs).

(C) The basis of enhancement of the thermal stabilities of the DNA-RNA duplexes by the 5'-tethered fluorophores

A recent report[18] by Hunter and Sanders shows that non-covalent interactions (π-π interactions) between aromatic systems are dictated by the surface-area, electrostatics, polarisability and the points of intermolecular contact of the aromatic systems in question. The most favourable conditions for π-π interactions is when both the interacting π-electron systems are electron-deficient, giving reduced π-electron repulsion[19].

In our earlier NMR study[10a] of 5'-tethered HPznm DNA-DNA duplex, the fluorophore was found to be stacked on the top of the terminal base pairs (which were C and G). In our current study, all the fluorophores can potentially stack in a similar manner with either the electron-deficient thymine base of the DNA-conjugate strand or the relatively electron-rich adenine base of the target strand depending on the nature of the π-orbital and their points of intermolecular contact[18]. Thus, we assumed that the strength of the π-π interactions between the fluorophore and the nucleobase would affect the thermal stability of the duplex.

We decreased the π-electron density of the Anth in **27** by replacing it with Pzn group in **19**. The resulting decrease in the π-electron repulsion between the fluorophore and the paired nucleobases (which are thymin-1-yl and adenin-9-yl) allows better π-π interactions between them. This manifests in the increase in the thermal stability ($\Delta\Delta T_m$ = 8.8° C, TABLE 1). Similarly, when the π-electron density is decreased by introduction of an exocyclic NO_2 substituent in NPhn, NPyr and DnPtd ring systems, an increase in the thermal stability is observed (compare thermal stabilities induced by DNA-conjugates **17**, **22** and **24** as compared to **16**, **21** and **23**, $\Delta\Delta T_m$ = 1.3-1.6° C, TABLE 1) due to a more favourable π-π interactions with the nucleobases. On the basis of the above observations documented under (ii) and (iii) in Section (B) (*vide supra*), it can be concluded that decreasing the π-electron density of a fluorophore tethered to a DNA enhances the thermal stability of its DNA-RNA duplex.

In our study, as the surface-area of the fluorophore is increased in going from Napth [α-Naph **25•29:** T_m = 22.9° C; β-Naph **26•29:** T_m = 23.4° C] to Phn [**16•29:** T_m = 26.9° C], an enhancement of the thermal stability of DNA-RNA duplexes is observed. However, further increase in the surface-area as in Pyr-linked **21** (T_m = 23.0° C) leads to a decrease in the thermal stability as compared to Phnbu-linked **18** (T_m = 25.9° C) with the same linker length. This is consistent with the proposal of Sanders and Hunter[18] that base-base stacking is usually associated with an offset rather than a face-to-face geometry, in which the strength of the π-π interaction does not depend on the surface-area of a stacker but on the active area of π-overlap.

TABLE 1 : The thermal stability (T_m[a] in °C) and the fluorescence enhancement data (ΔF[b]).

Entry #	9-mer conjugates 5'-X-TCCAAACAT-3'	10-mer RNA target 5'-rCAUGUUUGGA **(29)**			10-mer DNA target 5'-dCATGTTTGGA **(30)**			ΔF_{ss}[c]
		T_m	ΔT_m	ΔF[b]	T_m	ΔT_m	ΔF[b]	
1	**14** : Native DNA	20.3	-	-	26.2	-	-	-
2	**15** : Native RNA	33.3	13.0	-	25.2	-1.0	-	-
3	**16** : X = Phn	26.9	6.6	0.33	38.0	11.8	0.61	0.82
4	**17** : X = NPhn	28.2	7.9	1.02	40.0	13.8	0.88	0.79
5	**18 :** X = Phnbu	25.9	5.6	0.39	33.4	7.2	0.70	0.64
6	**19** : X = Pzn	29.9	9.6	0.82	37.7	11.5	1.13	0.68
7	**20 :** X = Pznm	27.1	6.8	0.32	36.5	10.3	0.24	n.d.
8	**21 :** X = Pyr	23.0	2.7	0.60	35.1	8.9	0.55	0.68
9	**22:** X = NPyr	24.6	4.3	1.02	33.7	7.5	1.15	0.76
10	**23** : X = Ptd	25.4	5.1	0.46	37.2	11.0	0.38	0.33
11	**24** : X = DnPtd	26.8	6.5	1.05	36.7	10.5	1.20	0.77
12	**25 :** X = α-Napth	22.9	2.6	12.70	32.3	6.1	11.80	0.66
13	**26 :** X = β-Napth	23.4	3.1	0.50	32.8	6.6	0.95	n.d.
14	**27 :** X = Anth	21.1	0.8	0.90	33.0	6.8	0.62	0.64
15	**28 :** X = Flo	21.0	0.7	1.50	31.0	4.8	1.10	0.71

[a] Error ± 0.4° C. ΔT_m values represent the change in T_m in the native ssDNA when conjugated with fluorophore. [b]ΔF gives the fluorescence enhancement measured as a ratio of the emission maxima for the conjugated duplex relative to the ssDNA conjugate. [c]ΔF_{ss} gives the ratio of the fluorescence enhancement measured as a ratio of the emission maxima for the ssDNA-conjugates at 55° C relative to 7° C. n.d. is not done. Protocol for the above measurements are given in the experimentals.

(D) Comparison of thermal stabilities of duplexes formed by 5'-tethered 9-mers 14-28 with RNA target 29 and DNA target 30

The salient features of the thermal stabilities of the duplexes formed by 5'-tethered 9-mers **14 - 28** with DNA target **30** has been reported[11]. Following are the characteristic differences which were observed due to 5'-fluorophore tethered 9-mer binding to a RNA target *viz-a-viz* DNA target (TABLE 1): (i) All fluorophores showed higher stability for conjugated DNA-DNA duplex (T_m = 31-40° C; ΔT_m = 5-14° C) as compared to conjugated DNA-RNA duplex (T_m = 21-30° C; ΔT_m = 1-10° C) (compare columns # 2 & 5 in TABLE 1).

(ii) Pzn, Phn and Ptd and their derivatives showed high duplex stabilisation for both conjugated DNA-DNA (T_m = 33-40° C; ΔT_m = 7-14° C) and conjugated DNA-RNA duplexes (T_m = 25-30° C; ΔT_m = 5-10° C). (iii) Pyr, Naph, Anth and Flo showed relatively lower duplex stabilisation for conjugated DNA-RNA duplexes (T_m = 21-25° C; ΔT_m = 1-5° C) as compared to conjugated DNA-DNA duplexes (T_m = 31-35° C; ΔT_m = 5-9° C). NPyr showed higher stability than Pyr for DNA-RNA duplex (Pyr **21•29:** T_m = 23.0° C; NPyr **22•29:** T_m = 24.6° C) whereas for DNA-DNA duplex it showed lower stability (Pyr **21•30:** T_m = 35.1° C; NPyr **22•30:** T_m = 33.7° C) . (iv) All fluorophores induced higher thermal stability in their conjugated hetero and homoduplexes, than in their respective native DNA-RNA duplex **14•29** (T_m = 20.3° C) and DNA-DNA duplex **14•30** (T_m = 26.2° C).

CD spectra *(vide infra)* of the heteroduplex **14•29** shows that it adopts the A-RNA form. In a heteroduplex, the DNA and RNA strands have been shown[10,20] to have two distinct backbone conformations: James and coworkers[20] have shown by NMR that in an antisense DNA-RNA hybrid duplex the deoxyribose undergo pucker transitions between South [$C_{2'}$-*endo* : $144° \leq P \leq 190°$; $\Psi_m = 38.6° \pm 3°$] and North conformation [$C_{3'}$-*endo*: $0° \leq P \leq 36°$; $\Psi_m = 38.6° \pm 3°$], whereas we showed[10] that the sugar moieties in the DNA strand had an intermediate conformation [$C_{1'}$-*exo*: $131° \leq P \leq 154°$; $\Psi_m = 39.6° \pm 5°$] between North and South forms in the HPznm-tethered DNA-RNA duplex. Hence, on binding to complementary RNA strand, the change in the sugar conformation of the DNA-conjugates **16-28** to a conformation undergoing pucker transitions between South and North domain alters the alignment of the sugar-phosphate backbone. This in turn affects the π-π interactions between the fluorophore and the nucleobase by influencing the proximity of the fluorophore with respect to the base. Since all fluorophores showed higher stabilisation for conjugated DNA-DNA duplex compared to conjugated DNA-RNA counterpart, it is likely that the former has a more intrinsic capability of stabilizing its structure by π-π interaction than in the latter.

(E) Fluorescence Studies

Fluorescence exhibited by any fluorophore tethered to a oligonucleotide is a cumulative effect of the electronic nature of the ligand, the strength of its interaction with the neighbouring bases[21], the nature of the tether[11], as well as the exposure of the ligand to the solvents and other solutes. The interaction of the fluorophore with the neighbouring bases is specific for each pair of fluorophore and nucleobase. The possible modes of interaction of a fluorophore in a oligo-conjugate DNA-DNA/RNA duplex is by intercalation, stacking or groove binding, which manifests through enhancement or quenching of the fluorescence. In our case, we anticipated it to be a π-π interaction.

Intercalative binding of the fluorophore is characterised by strong quenching and a red shift of the emission maxima as has been demonstrated for acridine labels attached to a terminal phosphate[2b,22,23], but the spatial origin of the interaction can not be correlated

unless an NMR or X-ray sructure is available. In this regard, a number of crystal and NMR structures have been reported[24] exhibiting the binding of different minor groove binders such as Netropsin, Distamycin, DAPI, $CDPI_3$ and Hoechst 33258 in free[24a-g] and tethered[25] states to duplex DNA. Of these ligands DAPI and Hoechst derivatives are moderately fluorescent in aqueous solution and show dramatic enhancement in quantum yields on binding to dsDNA[26]. For Hoechst 33258, the crystal structure of its A-T specific binding to dsDNA has been correlated to its intense increase in fluorescence on binding[27]. Based on the foregoing observations, when a ligand covalently linked to DNA showed an enhancement in the fluorescence upon duplex formation[12a], it was attributed to the minor groove binding.

Clearly, such correlation between fluorescence properties exhibited by tethered fluorophores and their mode of binding to duplexes and triplexes as determined from 3D structures makes fluorescence a more powerful tool for predicting local binding geometry for a variety of fluorophores.

(a) The correlation of changes in fluorescence with the local geometry as determined by NMR.

The moderate fluorescence quenching[11] of the fluorophore in the 5'-HPznm linked DNA-DNA duplex found in this work has been correlated with its NMR structure analysis[10a]: The NMR structure of 5'-HPznm linked DNA-DNA duplex showed that the fluorophore was indeed stacked on top of the terminal base pairs from the two complementary strands, while the 3'-dangling base lies out of the plain. The spatial orientation adopted by the HPznm fluorophore relative to the nucleobases in this homoduplex was the same as the one adopted by 3'-HPznm DNA-RNA heteroduplex[10b] (NMR). In the heteroduplex, the fluorophore is also planar, and stacked exterior to the terminal hydrogen-bonded nucleobases. Hence one would expect similar fluorescence behaviour from fluorophores stacked exterior to the terminal hydrogen-bonded nucleobases of the homo-[10a] and heteroduplex[10b]. In our previous study[11] using different fluorophores it was observed that the binding of the fluorophore to the exterior of the stacked heterocyclic bases was indicated by moderate quenching and little or no red shift of the emission maxima, and that was attributed to exteriorly stacked geometry of the fluorophore. Hence in the present work, similar quenching of fluorescence has been attributed to the exterior stacking of the fluorophore to the terminal nucleobase pairs.

(b) Fluorescence Studies on duplex conjugates.

In this work, fluorescence measurements were carried out at 7° C in 20 mM PO_4^{3-} buffer containing 1M NaCl at pH 7.3 for all 5'-fluorophore tethered ssDNA-conjugates **16** - **28** and their hetero and homoduplexes, and the results were compared (TABLE 1). This allowed us to evaluate the mode of interaction between the 5'-tethered-fluorophore and the adjacent nucleobases. For each fluorophore, the fluorescence intensity (FI) was measured for both the single strand conjugate and the double strand conjugate. The Fluorescence

enhancement (ΔF) was calculated[12a] as the ratio of FI in duplex state to FI in single strand state (FI for the single strand state was taken as 1.0). A comparison of ΔF values (TABLE 1) of DNA conjugates **17**, **19**, **22** & **24** with RNA target **29** and DNA target **30** shows marginal changes (ΔF ~ 0.8 - 1.2) implying only minute changes in the microenvironment of the fluorophore. Other DNA-conjugates showed the following deviations: (i) Phn-tethered 9-mer **16** showed notable quenching (ΔF ~ 0.3) with RNA target **29** and quenching (ΔF ~ 0.6) with DNA target **30**. Phnbu-tethered oligo **18** exhibited quenching on the similar lines with RNA target **29** (ΔF ~ 0.4) and DNA target **30** (ΔF ~ 0.7). (ii) The Pznm fluorophore **5** tethered to a 9-mer when complexes to targets **29** and **30** shows 3 to 4-fold quenching (ΔF ~ 0.3 and 0.24 respectively). (iii) Pyr-tethered 9-mer **21** and Ptd-tethered 9-mer **23** showed notable quenching with both RNA target **29** (Pyr: ΔF ~ 0.6; Ptd: ΔF ~ 0.5) and DNA target **30** (Pyr: ΔF ~ 0.55; Ptd: ΔF ~ 0.4). (iv) The α-Naph-tethered oligo **25** showed significant fluorescence enhancement with both targets **29** (ΔF ~ 12.7) and **30** (ΔF ~ 11.8). The β-Naph-tethered **26** however showed quenching with both targets **29** (ΔF ~ 0.5) and **30** (ΔF ~ 0.9). (v) Anth-tethered oligo **27** showed quenching (ΔF ~ 0.6) with DNA target **30** while Flo-tethered oligo **28** showed slight enhancement (ΔF ~ 1.5) with RNA target **29**.

We observed no shift in the emission maxima on comparing the single with the double stranded form for both DNA-DNA and DNA-RNA duplexes (TABLE 2) for all ssDNA-conjugates except **16** & **23**. In Phn-tethered DNA-conjugate **16**, the maxima observed at 365 nm for the single strand form was absent in the case of duplex with target RNA **29**. While both Ptd-linked **23** and α-Naph-tethered **25**, show a red shift on duplex formation with RNA target **29** (**23**: $\Delta Abs_{Em,max} \approx 7$ nm; **25**: $\Delta Abs_{Em,max} \approx 7$ nm) and DNA target **30** (**23**: $\Delta Abs_{Em,max} \approx 14$ nm; **25**: $\Delta Abs_{Em,max} \approx 3$ nm) as compared to the single strand state ($\Delta Abs_{Em,max}$ gives the shift in emission maxima on duplex formation).

On the basis of our fluorescence data, we can infer that the fluorophores **1- 9** & **11 - 13** show weak changes in ΔF values, suggesting stacking of the fluorophore onto the exterior of the ultimate heterocyclic base pairs. This has been confirmed for the Pznm-conjugated DNA-DNA duplex by comparison of NMR and fluorescence data in our earlier work[11]. The ssDNA-conjugate covalently linked to α-Napth **10** showed a dramatic enhancement in ΔF as normally observed for minor groove binders such as Hoechst 33258[12a].

In case of minor groove binder Hoechst 33258 a dramatic enhancement of fluorescence is observed on its binding to dsDNA in the minor groove, largely due to the protection of the dye in the excited state from nonradiative effects, presumably collisional processes involving water[26]. Moreover the hydrophobic environment of the minor groove also protects the dye from solvent molecules. A different scenario exsists with our tethered hetero & homoduplexes. With the exception of α-Napth, all other fluorophores tethered DNA-conjugates show moderate quenching or very weak enhancement. This could be due to increased collisions between the exposed surface of the stacked fluorophore and water

molecules.

TABLE 2 : The excitation and emission maxima (nm) of nonamer conjugates **16-28** in single strand state and as duplexes with the targets **29** & **30**.

Entry #	9-mer conjugates 5'-X-TCCAAACAT-3'	(λ_{Ex})	(λ_{Em}) Single Strand	(λ_{Em}) RNA Duplex	(λ_{Em}) DNA Duplex
1	**16** : X=Phn	304	365, 381	380	365, 379
2	**17** : X=NPhn	383	468	470	472
3	**18 :** X=Phnbu	354	382	380	380
4	**19** : X=Pzn	496	615	619	616
5	**20 :** X=Pznm	543	613	613	613
6	**21 :** X=Pyr	348	380	379	380
7	**22 :** X=NPyr	345	430	430	431
8	**23 :** X=Ptd	354	389	396	403
9	**24 :** X=DnPtd	330	419	419	423
10	**25 :** X=α-Napth	320	410	417	413
11	**26 :** X=β-Napth	327	414	415	414
12	**27 :** X=Anth	370	403	402	406
13	**28 :** X=Flo	304	407	404	407

(c) Fluorescence Studies on ssDNA-conjugates.

For ssDNA-conjugates **16-19**, **21-25**, **27** and **28**, we compared the FI of their respective emission maxima at 7° C and 55° C. We observed quenching (TABLE 1, $\Delta F_{ss} \sim 0.8 - 0.3$) for all of the conjugates with increase in temperature**.** The quenching of fluorescence of tethered fluorophores **1-4**, **6-10**, **12** & **13** can be interpreted as due to increased collisions with water molecules with the increase of temperature. This is also partly owing to disruption of the stacking of the fluorophore onto the ultimate base at the single strand level.

Decreasing the π-electron density of the fluorophore by nitration (as in NPhn, NPyr and DnPtd) resulted (see section B) in increased thermal stability ($\Delta\Delta T_m$ = 1.3-1.6° C, TABLE 1) of their heteroduplexes. Here it is found that at the ssDNA-conjugate level, similar decrease in the π-electron density of the fluorophore (as in NPhn, NPyr and DnPtd) brought about considerable fluorescence quenching, which was gauged by comparing the FI at emission maxima for each pair of nitrated/non-nitrated fluorophore linked to the 9-mer ssDNA at 7° C:

[$(FI)_{\mathbf{17}}$, Em max/$(FI)_{\mathbf{16}}$, Em max = 0.11; $(FI)_{\mathbf{22}}$, Em max/$(FI)_{\mathbf{21}}$, Em max = 0.14; $(FI)_{\mathbf{24}}$, Em max/$(FI)_{\mathbf{23}}$, Em max = 0.16]. In NPhn, NPyr and DnPtd tethered ssDNA-conjugate as compared to the non-nitrated counterparts, an increase in Stoke's shifts ($\Delta\lambda=\lambda_{Em}-\lambda_{Ex}$, where λ_{Em} and λ_{Ex} are emission and excitation maxima respectively) towards a higher wavelength were also observed: [$(\Delta\lambda)_{\mathbf{17}}$ - $(\Delta\lambda)_{\mathbf{16}}$ = 8 nm; $(\Delta\lambda)_{\mathbf{22}}$ - $(\Delta\lambda)_{\mathbf{21}}$ = 53 nm; $(\Delta\lambda)_{\mathbf{20}}$ - $(\Delta\lambda)_{\mathbf{23}}$ = 55 nm]. On similar lines, fluorescence quenching and increase in Stoke's shifts were also observed in the heteroduplex state at 7° C for each pair of nitrated/non-nitrated fluorophore: [$(FI)_{\mathbf{17\bullet29}}$, Em max/$(FI)_{\mathbf{16\bullet29}}$, Em max = 0.49; $(FI)_{\mathbf{22\bullet29}}$, Em max/$(FI)_{\mathbf{21\bullet29}}$, Em max = 0.32; $(FI)_{\mathbf{24\bullet29}}$, Em max/$(FI)_{\mathbf{23\bullet29}}$, Em max = 0.39] and [$(\Delta\lambda)_{\mathbf{17\bullet29}}$ - $(\Delta\lambda)_{\mathbf{16\bullet29}}$ = 11 nm; $(\Delta\lambda)_{\mathbf{22\bullet29}}$ - $(\Delta\lambda)_{\mathbf{21\bullet29}}$ = 64 nm; $(\Delta\lambda)_{\mathbf{24\bullet29}}$ - $(\Delta\lambda)_{\mathbf{23\bullet29}}$ = 64 nm]. Consistent with our earlier NMR studies[10] on tethered homo and heteroduplexes, we conclude that both at the single-strand and double strand level, decreasing the π-electron density of the fluorophores by nitration, enhanced the π-π interaction (*i.e.* enhanced base stacking[18]) between the fluorophores and the adjacent nucleobases which was manifested in fluorescence quenching.

(E) Circular Dichroism (CD) experiments

We have been interested to explore the effect of different tethered-fluorophores on the structure of ssDNA as well as on the overall structure of their duplexes with DNA and RNA targets by studying the change in the chiral environment as compared with the native oligo counterpart.

CD exploits ellipticity, the differential absorption of left- and right-handed circularly polarized light. Ellipticity depends on relative spatial orientations of a molecule's different parts and its overall organization. In nucleic acids, ellipticity is modulated by disorientation or reorientation of the nucleobases with respect to each other. The chirality inherent in the nucleoside gets amplified at the oligomer level, making structural transitions in nucleic acids

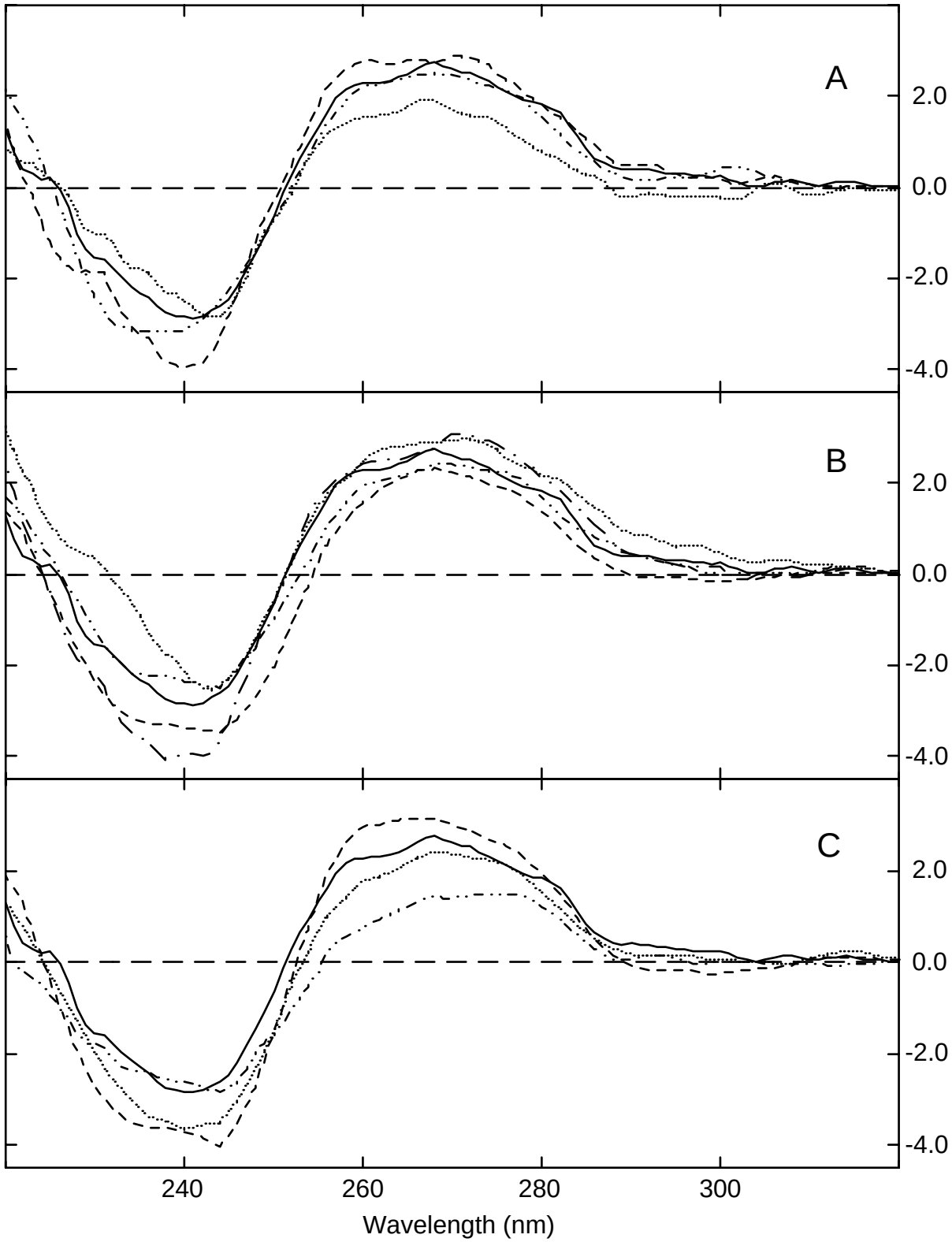

FIG. 2 : CD spectra of duplexes of ssDNA-conjugates with DNA target **30** as a function of wavelength (nm). Panel **A**: **16•30** (– · · –), **17•30** (– – – –), **19•30** (·····); Panel **B**: **21•30** (·····), **22•30** (– · · –), **23•30** (__ · __), **25•30** (– – – –); Panel **C**: **18•30** (– – – –), **27•30** (– · · –), **28•30** (·····). CD spectras of non-modified duplex DNA-DNA **14•30** (————) is shown in each panel for comparison.

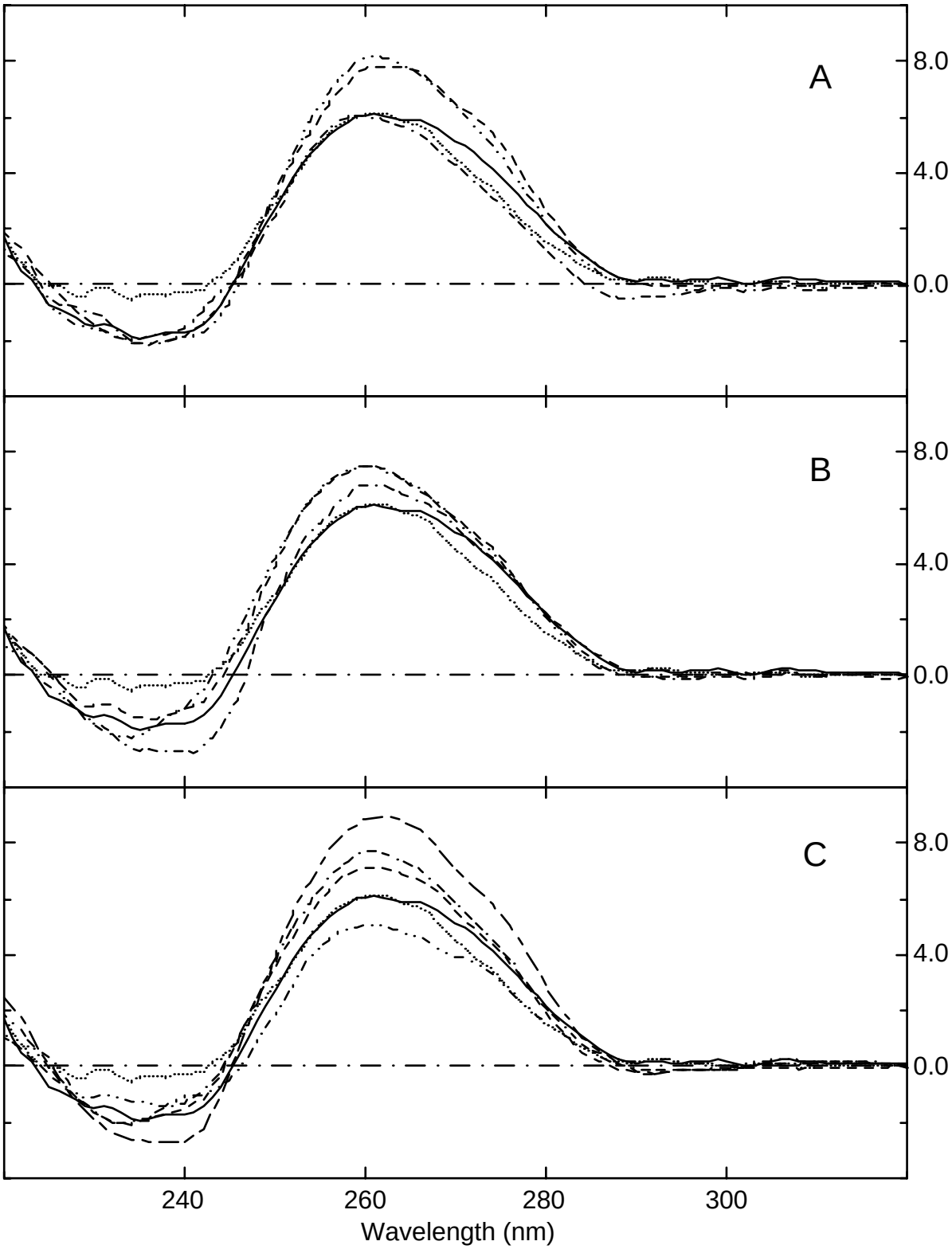

FIG. 3 : CD spectra of duplexes of ssDNA-conjugates with RNA target **29** as a function of wavelength (nm). Panel **A**: **16•29**(– – – –), **17•29**(– · · –), **19•29**(– – · – –); Panel **B**: **21•29**(– – – –), **22•29**(– · · –), **23•29**(– – · – –); Panel **C**: **18•29**(__ – __), **25•29**(– – – –), **27•29** (– · · –), **28•29**(– – · – –). CD spectras of non-modified duplexes DNA-RNA **14•29** (————) and RNA-RNA **15•29** (·····) are shown in each panel for comparison.

TABLE 3. CD spectral differences (as RMS values)[a] for different 5'-conjugated DNA-DNA and DNA-RNA duplexes as compared to non-modified DNA-DNA (DD), DNA-RNA (DR) & RNA-RNA (RR) duplexes.

Entry #	9-mer conjugates 5'-X-TCCAAACAT-3'	conjugated DNA-DNA (cDD)			conjugated DNA-RNA (cDR)			conjugated ssDNA (cD)	
		$CD_{(cDD)}$-$CD_{(DD)}$	$CD_{(cDD)}$-$CD_{(DR)}$	$CD_{(cDD)}$-$CD_{(RR)}$	$CD_{(cDR)}$-$CD_{(DD)}$	$CD_{(cDR)}$-$CD_{(DR)}$	$CD_{(cDR)}$-$CD_{(RR)}$	$CD_{(cD,55)}$-$CD_{(cD,7)}$	$CD_{(cD,55)}$-$CD_{(D,55)}$
1	**14** : X=None	-	1.82	1.94	1.82	-	0.63	1.08	-
2	**16** : X=Phn	0.57	2.30	2.33	1.66	0.96	1.20	0.34	0.82
3	**17** : X=NPhn	0.48	1.76	2.00	2.49	0.77	1.12	0.37	0.89
4	**18 :** X=Phnbu	0.69	1.98	2.23	2.92	1.25	1.59	0.62	1.03
5	**19** : X=Pzn	0.52	2.16	2.17	1.74	0.52	0.59	0.32	0.89
6	**21 :** X=Pyr	0.73	1.83	1.84	2.42	0.64	0.80	0.50	0.71
7	**22:** X=Npyr	0.32	1.99	2.06	2.46	0.69	0.89	0.64	0.34
8	**23** : X=Ptd	0.58	1.90	2.17	1.93	0.49	1.00	0.98	0.79
9	**25 :** X=α-Napth	0.64	2.32	2.48	2.25	0.50	0.79	0.98	0.57
10	**27 :** X=Anth	0.76	2.50	2.57	1.36	0.64	0.62	0.52	0.49
11	**28 :** X=Flo	0.49	2.19	2.36	2.43	0.66	0.89	0.38	1.06

[a]Numbers are RMS values = $\{\Sigma_\lambda[CD(\lambda)_1 - CD(\lambda)_2]^2/n\}^{1/2}$ (in $M^{-1}cm^{-1}$), where the differences between the CD values of spectra 1 and 2, i.e. $CD(\lambda)_1$ and $CD(\lambda)_2$ were squared and summed over n wavelengths; then the square root was taken. The number of wavelengths, n, was 101 (320-220).

visible to CD. Hence changes in its asymmetry and order are translated into the changes in the observed ellipticity. A recent report[28] shows change in ellipticity as a more reliable measure of monitoring nucleic acid structural transitions than hyperchromicity. Although CD spectra does not give detailed spectral information on local structure, it provides information about the global conformation of the conjugated DNA-RNA and DNA-DNA duplexes, specially compared to unmodified RNA-RNA and DNA-DNA duplexes (used as reference A-form and B-form for RMS calculations).

(a) CD Studies on duplex conjugates.

The CD spectra of duplexes of DNA conjugates **16**-**19**, **21**-**23**, **25**, **27** & **28** with RNA target **29** and DNA target **30** were recorded (Figs. 2 & 3) at 10° C. The CD spectra of the unmodified DNA-DNA, DNA-RNA and RNA-RNA duplexes were also recorded as reference for comparison. To further quantify the differences between each conjugated DNA-target duplex and the unmodified DNA-DNA, DNA-RNA and RNA-RNA duplexes, RMS

values[29] between each pairs of CD spectra were calculated (TABLE 3).

The CD spectra (FIG. 2) of DNA conjugates **16-19**, **21-23**, **25**, **27** & **28** with DNA target **30** were very similar to the unmodified DNA-DNA duplex, which were evident from comparable positive and negative molar ellipticity of moderate magnitude at wavelengths above 220 nm and a crossover point between 208 nm and 262 nm, characteristic of the B-DNA conformation[30]. On comparing the RMS values (TABLE 3), we arrived at the conclusion that tethering the DNA with different fluorophores did not make any gross changes in the helical structure of the conjugated DNA-DNA duplex. Interestingly, these fluorophores, on the other hand, enhance the thermal stability of these duplexes (ΔT_m = 5-14° C).

The CD spectra (FIG. 3) of DNA conjugates **16-19**, **21-23**, **25**, **27** & **28** with RNA target **29** showed that the conformation taken up by these heteroduplexes is more characteristic of A-RNA conformation showing a large positive molar ellipticity above 260 nm. This was also concluded by comparing the RMS values in TABLE 3 which shows that these hybrid duplexes show conformationcloser to the A-form RNA-RNA duplex, or more like the unmodified DNA-RNA duplex. Hence it can be concluded that in the conjugated heteroduplexes, no gross change in the helical structure was observed with covalent linkage of the fluorophore despite the enhancement of duplex thermal stability (ΔT_m = 1-10° C).

(b) Comparison of the NMR structure and the CD data.

In our earlier NMR work[10a], we have shown that as the stability of the DNA-DNA duplex increases in the matched duplex compared to the mismatched counterpart, the exchange rates of the imino protons as well as the water activity (hydration level) in the minor and major groove decreases considerably in the former. It has been shown[31] that the energy of activation (E_a) of the exchange process of imino protons with the bulk water is the highest in the core part of both the DNA-DNA[31a,b] and DNA-RNA[31c] duplexes, which decreases step-by-step towards the terminal base pair. The imino protons for the terminal base pairs in the native DNA-DNA[10a,31a,b] and DNA-RNA[10b,31c] duplex are not normally observed due to rapid exchange with the bulk water. However, the introduction of a 5'-HPznm tethered fluorophore in a DNA duplex has been shown to slow down the exchange rate of the terminal imino protons with the bulk water, making it observable in the NMR time scale[10a,31a]. Similarly, the introduction of a 3'-HPznm tether in a DNA-RNA duplex not only enhances its stability compared to the native counterpart, but also makes the imino protons for the terminal base pair observable in the NMR[10b,31c]. Thus the attachment of the fluorophore at the 3'- or 5'-end of a DNA-DNA or DNA-RNA duplex results in the increase of E_a of the exchange of the terminal base pair imino protons[31] compared to the native counterpart. This stabilisation of the H-bonds of the terminal base pair is owing both to the stacking and hydrophobic effects of the terminal tethered fluorophore with the adjacent nucleobases which reduces the water availability[31] around the terminal imino proton, thereby leading to an increase in the thermal

stability of both hetero and homoduplexes (TABLE 1).

In this work the differences observed in the CD spectra (Figs. 2 & 3) of the duplexes of ssDNA-conjugates **16**-**19**, **21**-**23**, **25**, **27** or **28** with targets **29** or **30** as compared to their native counterparts, is attributed to only small changes in the base stacking with the fluorophore. This implies that the helicity of the core of the duplex remains more or less unaltered as a result of tethering with different fluorophores. Consistent with our earlier NMR observation on HPznm tethered DNA-DNA[10a,31a,b] and DNA-RNA duplexes[10b,31c], the increase in the thermal stability (TABLE 1) of all tethered duplexes studied here results from the increased hydrophobicity and decreased water availability owing to the stacking interaction of the tethered-fluorophore with the adjacent nucleobases, which in turn stabilizes the H-bonding of the terminal base pair.

(c) CD Studies on ssDNA-conjugates.

CD spectra for non-aggregated ssDNA has been earlier reported[28,32]. In this paper, CD spectra has been recorded from 320 nm to 220 nm on ssDNA **14**, **16**-**19**, **21**-**23**, **25**, **27** & **28** at 7° C and 55° C (FIG. 4). To quantify the observed differences in the CD spectra of each oligo at 7° and 55° C, the CD spectral differences (as RMS values)[29] were calculated (TABLE 3). On heating, the natural 9-mer DNA **14** showed the highest spectral difference as evident from an RMS value of 1.08 (the lowest being RMS = 0 for no deviation), implying disruption of the order and change in relative orientation of the nucleobases in the ssDNA with increase in temperature.

CD spectral differences shown by ssDNA-conjugates **16** (0.34), **17** (0.37), **18** (0.62), **19** (0.32), **21** (0.50), **22** (0.6), **27** (0.52) & **28** (0.38) were comparatively lower. Oligo **23** (0.98) & **25** (0.98) showed similar change in RMS values as the natural 9-mer **14**. The level of disruption of stacking (order) with increase in temperature in the ssDNA-conjugates was in general lower than that observed for the native ssDNA **14**, implying that the fluorophore is assisting in maintaining the order and asymmetry even at the higher temperature.

The CD spectral differences between ssDNA-conjugates at 55° C and ssDNA **14** at 55° C were also calculated. All DNA-conjugates showed spectral differences (TABLE 3) from the CD spectra of 9-mer DNA **14** at 55° C, but the spectral differences shown were closer to their respective structures at 7° C (FIG. 4). This data corroborates our above statement that increase in temperature has less influence on the structure of ssDNA-conjugates than in the non-tethered counterpart because the fluorophore assists in maintaining single strand order through π-π interaction with the last nucleobase in the former. This is consistent with the finding[33] that the naphthyl-adenine stacking in a dimer was much less disrupted up to 88°C compared to stackings in adenine-adenine or naphthyl-naphthyl dimer.

(d) Conformational Pre-organization of the ssDNA-conjugates.

Does the ssDNA have a random coil like structure or is it pre-organized into a

conformation close to the helical structure? It is known that ssDNA can exhibit intramolecular

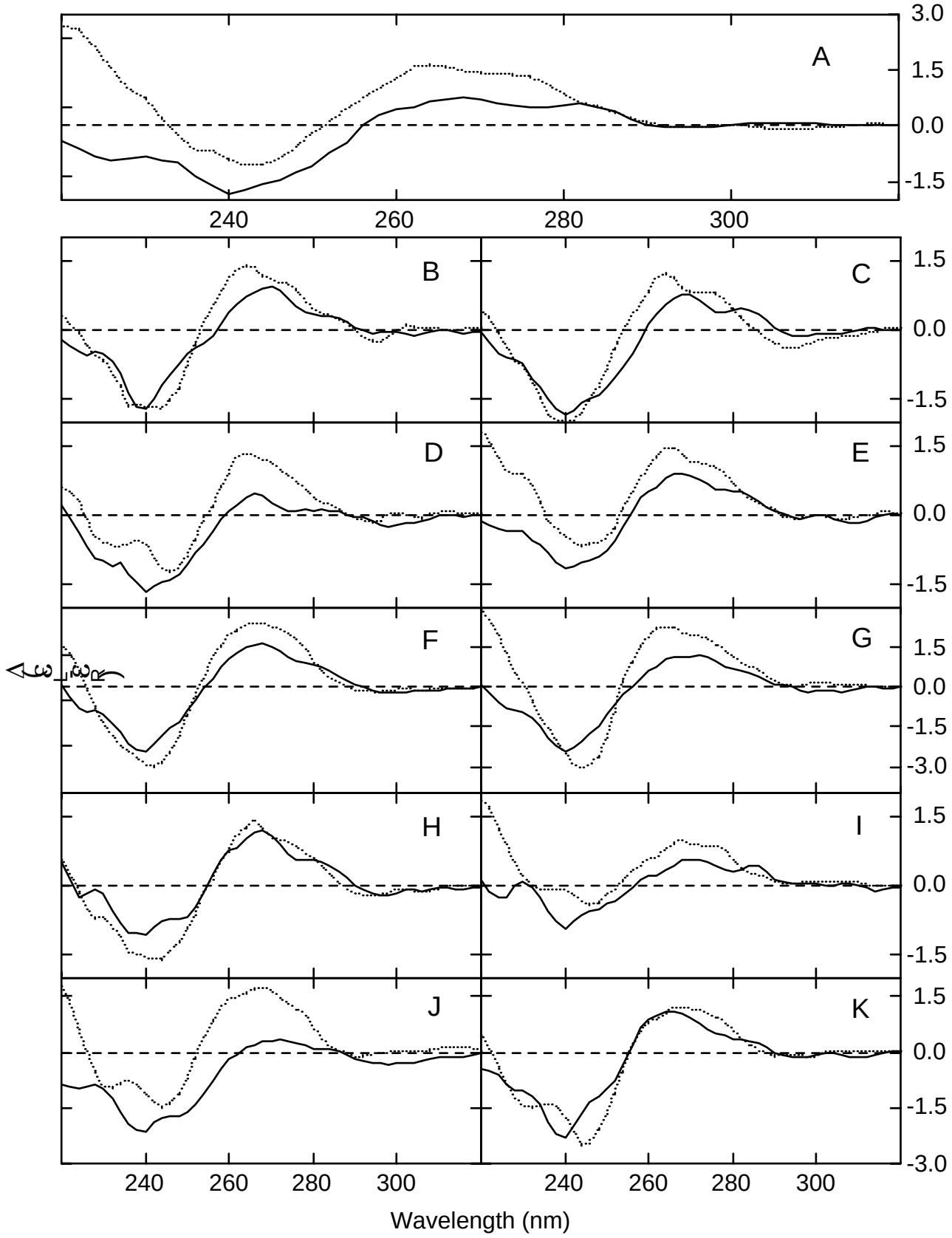

FIG. 4 : CD spectra of ssDNA-conjugates at 7° C (·····) and 55° C (————) as a function of wavwlength (nm). Panel **A**: **14**, Panel **B**: **16**, Panel **C**: **17**, Panel **D**: **21**, Panel **E**: **22**, Panel **F**: **18**, Panel

G: **23**, Panel **H**: **19**, Panel **I**: **27**, Panel **J**: **25** and Panel **K**: **28**.

interactions that poise them for duplex formation in enthalpically favourable manner[34]. These interactions comprise of a large exothermic intramolecular base stacking which balances the large negative entropy change in ordering the nucleotide backbone. The resulting free-energy change is small, hence permitting readily reversible associations by the ssDNA[35].

The CD data presented above suggests that it is possible for the ssDNA to adopt a pre-organized helical conformation which is indeed assisted by tethering an aromatic π-stacker at the terminus. The π-π interaction between the tethered-fluorophore (π-stacker) and the adjacent nucleobase is stronger in our ssDNA-conjugate than between two natural nucleobases[10a] in the native ssDNA counterpart, thereby augmenting the vertical base-base interactions in the former. This is consistent with the fact that a dangling nucleobase does not stabilize the last base pair to an extent that a tethered fluorophore does[10a]. This presumably makes the free energy of pre-organization of the fluorophore tethered ssDNA more favourable enthalpically than the native counterpart. This is supported by the observation[33] that the stacking propensity between adenine and naphthyl group is stronger in an adenine-naphthyl dimer than between two adenine moieties in an adenine-adenine dimer.

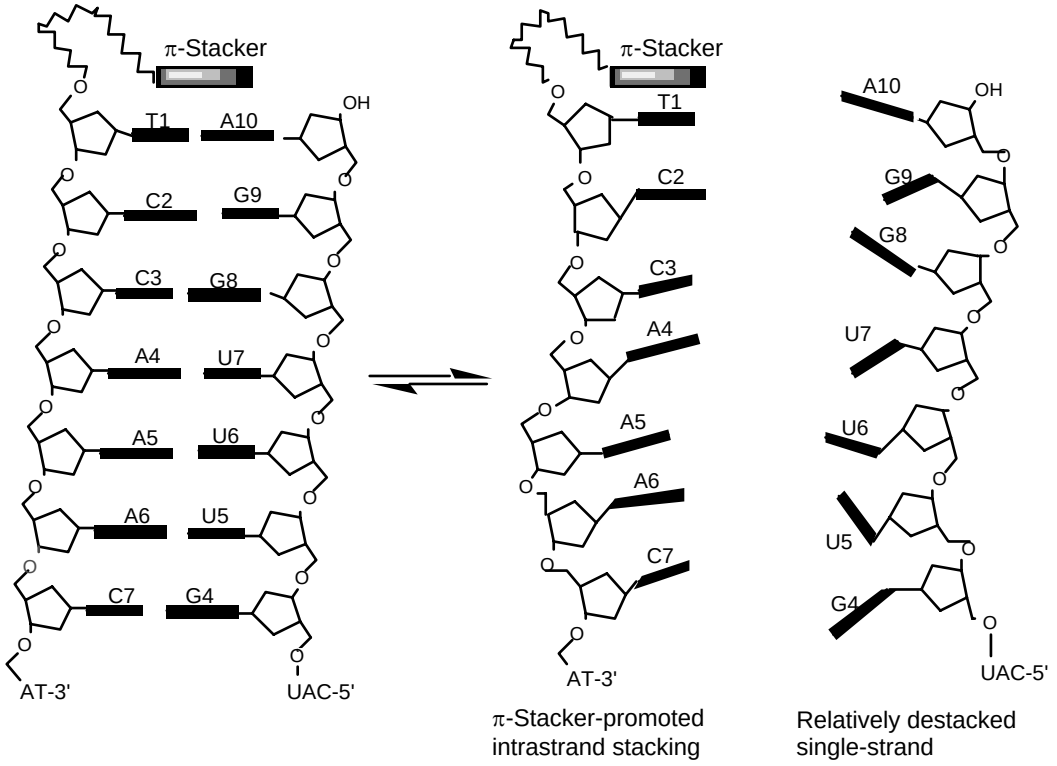

FIG. 5. Illustration showing a π-stacker covalently linked to the 5'-terminus of a ssDNA-conjugate assisting in the pre-organization by assisting in the π-π stacking, thereby reducing the population of random coil structures. Also shown enhancment of stability of a duplex with a target RNA strand by stabilization of terminal H-bonds by the π-stacker.

We were not able to observe any single strand melting such as those observed by Vesnaver and Breslauer for ssDNA[34], except for the fact that a steady increase (~10 % in the temperature range used) in the UV absorbance of ssDNAs **14**, **16-19**, **21-23**, **25**, **27** & **28** was seen with increase in temperature in the range 2-80° C. This is consistent with a known fact that UV absorbance spectroscopy often fails to detect structural change in nucleic acid, which is however observable by CD[28]. The CD spectra for ssDNA-conjugates (FIG. 4) show more decreased band intensities (RMS value change of 0.3 - 0.6 in going from 7-55°C) compared to the native **14** as well as for **23** and **25** (RMS = 1.0) from 320 to 220 nm, indicating more resistance to the facile melting behaviour of the stacked structure in the former compared to the latter. This observation clearly indicates that the 5'-tethered fluorophore is assisting in maintaining order and asymmetry in ssDNA-conjugates (FIG. 5).

(F) RNase H hydrolysis.

The mechanism of antisense effects of oligo-DNA and their analogues involve either RNase H mediated cleavage[36] of the RNA strand in the hybrid duplex, or the physical blocking of the translation machinery[37].

RNase H is an enzyme that selectively recognizes a (3'→5')-RNA-DNA heteroduplex and hydrolyzes the RNA strand of the heteroduplex[38] to produce a 3'-hydroxyl termini and a 5'-phosphate at the point of cleavage[39]. RNase H possesses both endo- and 3'→5' exonuclease activities[40]. A DNA-RNA duplex of 4-6 bp length is known to be adequate to evoke RNase H activity[41]. This was demonstrated by RNase H digestion of heteroduplexes between RNA and chimeric ODN comprising of native phosphodiesters sandwiched between phosphate analogues not eliciting RNase H cleavage on their own. Only heteroduplexes in which the chimeric ODN had 4-6 bp with native phosphodiesters exhibited cleavage by RNase H. Hence our tethered short heteroduplexes of 9 bp length (*i.e.* DNA-conjugates **17**, **19**, **21**, **23** & **27** with RNA target **29**) were deemed to be good candidates to examine if they activate RNase H.

TABLE 4. Kinetics of RNase H cleavage of different 5'-tethered DNA-RNA duplexes and competitive inhibition of the RNase H cleavage by 5'-Ptd DNA-DNA duplex

	Non-mod DNA-RNA **14•29**	5'-NPhn DNA-RNA **17•29**	5'-Pzn DNA-RNA **19•29**	5'-Pyr DNA-RNA **21•29**	5'-Ptd DNA-RNA **23•29**	5'-Anth DNA-RNA **27•29**
$t_{50\%}$[a] (min)	79.5	89.3	72.6	103.0	68.9	151.4
$t_{99\%}$[b] (min)	201.0	207.3	206.2	263.8	281.5	483.51
%(cleavage)$_{inhibit}$[c]	6.0	50.0	23.4	17.2	21.0	13.6

[a]half-life of cleavage of RNA strand by RNase H. [b]lifetime of completion of cleavage. [c]implies observed cleavage (expressed as percentage) of different 5'-tethered DNA-RNA duplexes by RNase H inhibited by 5'-Ptd DNA-DNA duplex relative to cleavage by uninhibited RNase H.

We subjected the heteroduplexes formed by mixing the DNA-conjugates **17**, **19**, **21**, **23** & **27** with RNA target **29** under reported conditions[42] to observe if RNase H hydrolyses the RNA strand of the heteroduplexes. For comparison, we also tested the native heteroduplex under the same condition for RNase H activation. The RNA strand in all heteroduplexes showed hydrolysis by RNase H which was monitored by recording the changes in UV absorbance at 260 nm at 20° C (see experimental section)[43].

We have correlated the T_m data (TABLE 1) and the RMS values (TABLE 3) of the heteroduplexes with the half-life ($t_{50\%}$) and the lifetime of completion ($t_{99\%}$) (TABLE 4) of DNA-conjugates assisted RNA excision by RNase H. The results of our studies are as follows:

(i) Heteroduplexes tethered with fluorophores like Pzn and Ptd had the shotest half-life of digestion by RNase H (TABLE 4, row 1). This was owing to higher thermal stability (ΔT_m = 5-10° C) and least deviation of the global structure from the native heteroduplex. The latter can be gauged by comparing the CD spectral differences shown by heteroduplexes tethered with Pzn (RMS value = 0.52) and Ptd (RMS value = 0.49) as compared to the other fluorophores used in the study.(ii) NPhn tethered heteroduplexes showed a longer half-life ($t_{50\%}$ = 89.3 min) of RNA excision by RNase H, although NPhn group stabilizes the heteroduplex substantially (ΔT_m = 8° C). The advantage gained by thermal stability is offset by a greater deviation from the native heteroduplex [clearly seen by a higher RMS value = 0.77 (TABLE 3, column 5)].

(iii) Pyr and Anth tethered heteroduplexes show much a longer half-life (TABLE 4, row 1) owing to lower stability (ΔT_m = 1-3° C) and a greater deviation (TABLE 3, column 5) from the native heteroduplex.

(iv) It is known that a DNA-RNA heteroduplex in general adopts A-form geometry, but the conformation can vary from A- to B-form depending on the sequence[44]. To see if a pure B-form, *i.e.* a DNA-DNA duplex, inhibits the binding and digestion of A-form DNA-RNA duplex by RNase H, competitive inhibition experiment of the RNase H was performed: In these experiments, we allowed the possible capture of a native DNA-DNA duplex or a conjugated DNA-DNA duplex by RNase H for 10 min at 20° C. Then a native DNA-RNA duplex or a conjugated DNA-RNA duplex was introduced in the above solution. TABLE 4 shows the percentage cleavage of different heteroduplexes in the presence of 5'-Ptd tethered DNA-DNA duplex (**23•30**) by RNase H. In general, about 10-20 % cleavage of the heteroduplex was observed in presence of DNA-DNA duplex, as compared to the case where no DNA-DNA duplex was present.

CONCLUSION

Studying the thermal stability, fluorescence, CD and RNase H cleavage characteristics of 5'-fluorophore tethered DNA-RNA duplexes and comparing these with their corresponding

DNA-DNA duplexes led to the following conclusions:

(1) Fluorophores **1-13** when covalently linked to the 5'-terminus of ssDNA oligonucleotides **16-28** respectively, enhance their affinity to both RNA (**29**) and DNA (**30**) targets, relative to the native counterparts. Using these DNA-conjugates, we were able to show predictable influence of changing bulk and π-electron density of the 5'-tethered fluorophore on the thermal stability and fluorescence characteristics of DNA-RNA and DNA-DNA duplexes. The tethered homoduplexes displayed higher stability than the heteroduplexes.

(2) Decreasing the π-electron density of the fluorophores by both endocyclic modification (by replacing Anth by Pzn) and exocyclic modification (by nitrating Phn, Pyr & Ptd) leads to an enhancement of the thermal stability of their conjugated DNA-RNA duplex. This has been attributed to a more favourable π-π interaction between the fluorophore and the nucleobase following the model given on the nature of π-π interactions by Sanders and Hunter[18]. This model also explains our observation that increasing the surface-area of 5'-stacker only increases the thermal stability of the duplex, if it leads to an increase in the area of π-overlap between the 5'-stacker and the adjacent nucleobase.

(3) Fluorophores such as Phn (**1**), NPhn (**2**), Phnbu (**3**), Pzn (**4**), Pznm (**5**), Pyr (**6**), Ptd (**8**), β-Napth (**11**) and Anth (**12**) when tethered to ssDNA showed quenching on duplex formation. Also NPyr (**7**), DnPtd (**9**) and Flo (**13**) show slight or no enhancement in fluorescence yields. These small changes in fluorescent intensity suggest stacking of the fluorophore on the exterior of the ultimate heterocyclic base pairs. 5'-tethered α-Napth (**25**) shows dramatic enhancement in fluorescence as normally observed for the minor groove binders, suggesting that the spatial environment of 5'-tethered α-Napth in **25** is quite different from the other 5'-tethered fluorophores.

(4) The enhancement of heteroduplex stability by nitrated ssDNA-conjugates as compared to the non-nitrated counterparts, owing to increased fluorophore-nucleobase π-π interaction, is visible at the level of ssDNA-conjugates and their heteroduplexes through the observed relative fluorescence quenching of the nitrated fluorophore. This result is consistent with our earlier NMR studies on tethered homo[10a] and heteroduplexes[10b] and has been interpreted as owing to the enhanced exterior stacking.

(5) Our CD data shows that tethering the DNA with different fluorophores did not make any gross changes in the helical structure of the duplexes of DNA-conjugates with RNA and DNA targets although it leads to an increase in the thermal stability of these duplexes. The fluorophore assists in preorganising the ssDNA-conjugates into a helical conformation and induces more efficient H-bonding at the terminal base pairs as well as reduces hydration level in the core of the duplex in general, which manifests itself in a higher thermal stability of the duplex.

(6) Here all conjugated DNA-RNA duplexes tested, showed positive RNase H activation. The RNase H activation decreased with lower thermal stability (T_m) of the heteroduplex and greater deviation from the structure of the native DNA-RNA duplex of the same sequence.

Hence this shows that data from CD and T_m studies would be useful in prediction of good antisense compounds.

(7) A report[45] which was recently published during the progress of this work showed that a fluoro-arabinonucleic acids (2'F-ANA)-RNA duplex showed a close CD resemblence to the native DNA-RNA counterpart, leading to similar susceptibility to RNase H. In contrast, a 2'F-RNA-RNA duplex was not digested at all as the native RNA-RNA counterpart. This study showed that a lower thermal stability of the duplexes (such as ANA-RNA duplex) translated into poorer digestion by RNase H, whereas 2'F-ANA-RNA, DNA-RNA, DNA-thioate-RNA hybrids had higher stabilities, and were cleaved faster. This work is consistent with ours in that an effective antisense ON should have a DNA-type conformation in the resulting antisense ON-RNA duplex, and higher the stability, the faster is the cleavage by RNase H.

(8) It has been herein shown that the 5'-tethered planar aromatic moieties can help in the pre-organization of ssDNA by strengthening intrastrand base stacking[46], thereby implying that the 5'-fluorophore tethered ssDNA has relatively less random coil structure compared to the native counterpart (FIG. 5), which assists in the self-assembly process of a conjugated DNA-DNA duplex. The free energy of duplex formation between a DNA with a stacker at its terminus and its complementary target is much lower than one between a native DNA and its target. This is also substantiated by the observation by Kool and Matray[47] where inserting a pyrene-abasic pair into a DNA duplex decreases its free energy. The conjugated DNA-target duplex formation can be visualized as a two step process. The first step is of pre-organization, *i.e.* the π-π interaction between the 5'-tethered stacker and the adjacent nucleobase is propagated along the single strand through vertical base-base interaction as in the native DNA[34,35,46]; note however that the 5'-tethered stacker-base interaction is stronger than the native base-base stacking[33]. This 5'-stacker-base interaction aligns the ssDNA-conjugate into a more ordered conformation. The decrease in entropy due to pre-organization here is offset by the increase of enthalpy of both fluorophore-base and base-base stacking (π-π interaction) to give a favourable free energy change. The second step involves the formation of H-bonds between each pair of complementary nucleobases and the formation of the helix[35,46]. Here the 5'-fluorophore plays an unique role by increasing hydrophobicity and decreasing water availability, thereby stabilizing the terminal H-bonds enthalpically as observed by NMR[10,31].

EXPERIMENTAL SECTION

The synthesis of oligonucleotides **14**, **16 - 22**, **25 - 28** have been reported in an earlier work[11]. The synthesis, deprotection and purification of oligonucleotides **23** and **24** were performed as reported in our earlier work[11]. The 9-mer RNA **15** and 10-mer RNA **29** were synthesised, deprotected and purified by HPLC using reported procedures[48].

A Gilson equipment with Pump Model 303, Manometric Module Model 802C and Dynamic Mixer 811B connected to a Dynamax computer program for gradient control was used for semi-preparative RP-HPLC separations on Spherisorb 5ODS2. Melting

measurements were carried out using a PC-computer interfaced Perkin Elmer UV/VIS spectrophotometer Lambda 40 with PTP-6 peltier temperature controller. Fluorescence measurements were carried out using an Aminco SPF-500 Corrected Spectra Spectrofluorometer or a Hitachi F-4000 Spectrofluorometer with a Xenon lamp power supply. The CD spectra were recorded using a JASCO J41-A Spectropolarimeter.

Physico-chemical measurements. For all measurements, the oligonucleotide solutions were heated to 70° C for 3 min and then allowed to cool down to 20°C for 30 min. They were equilibrated overnight at 4° C.

Melting measurements. UV melting profiles were obtained by scanning A_{260} absorbance versus temperature with a heating rate of 1.0° C / min. The T_ms values were calculated from the culmination point of the first derivative of the melting curves with an accuracy of ±0.4° C. The error in the UV measurements was the deviation observed from the averaged T_m value of four experiments done on the duplex 19•30 under identical conditions (*i.e.* buffer sample concentration, sample preparation and incubation, and rate of heating). The duplex melting experiments were carried out in buffer A: 20 mM Na_2HPO_4 / NaH_2PO_4, 0.1M NaCl at pH 7.3 The extinction coefficients for oligonucleotides **14 - 30** were calculated with the nearest-neighbour approximation[49]. In the cases of the tethered oligomers (**16-28**), the contribution of the aromatic moieties towards their extinction coefficients at 260 nm were estimated from the UV spectra of 1μmol solutions of polyarenes **1-13**.

In a duplex melting measurement, where 1μM of each single strand was used, 1.3 nmol of target sequence (**29**, 0.134 OD / 10 μl H_2O), (**30**, 0.126 OD / 10 μl H_2O) and 1.3 nmol of nonamer sequence (0.116 OD / 10 or 20 μl H_2O) were added to 1260 ml of buffer (20.64 mM Na_2HPO_4 / NaH_2PO_4, 0.1032 M NaCl, pH 7.3), giving, after dilution with water to 1.3 ml, concentrations of ~1μM of each oligomer and the precise buffer concentration. For the heteroduplexes which displayed T_ms values in the range 20 - 33 ° C (entries # 1-15, TABLE 1), the melting curves and dissociation T_m were measured in the temperature range 10 - 55° C. While for homoduplexes[11] (T_ms values ~ 25 - 40 ° C, TABLE 1) the temperature range used was 15 - 60 ° C. At their respective starting temperature, the complete complexations of the hetero and homoduplexes was verified from the baseline of the melting curves having approximately zero slope, suggesting that the sample is in >98% in complexed form, except for the duplex **20•29,** which was >95% in the duplex form.

Fluorescence. For the fluorescence measurements, the concentration of each oligomer was set to 0.02 abs. units at the excitation maxima (TABLE 2) for each fluorophores in 1.3 ml of buffer B (20 mM Na_2HPO_4 / NaH_2PO_4, 1.0M NaCl, pH 7.3). The ratio of the single strands in the mixtures of duplexes was always 1:1. During measurements the temperature was kept at ~10° C by circulating termostated water through the cuvette holder. Relative fluorescence intensities and Stoke's shifts were determined for each sample at the same excitation/emission bandpass width.

Circular Dichroism Spectra. All CD experiments were recorded from 320 to 220 nm in 0.2 cm path length cuvettes using 10.4 μM strand concentration in 600 μl of buffer B. For CD spectra of the duplexes the temperature was maintained at 10° C by circulating termostated water through the cuvette holder, while for ssDNA-conjugates it was maintained at 7° C and 55° C. The samples were equilibrated at the required temperature for 10 min before recording the spectra. Each spectrum was an average of two scans with the buffer blank subtracted, which was also an average of two scans at the same scan speed (10 nm/min). The time constant and the sensitivity used were 16 sec and 20 x 10^{-2} m°/cm respectively. Each point in

the spectra was manually fed into the Profit software in a Macintosh, where the spectra was smoothened using a 3-point average. The CD spectra was converted to $\Delta\varepsilon$ and reported as per mole of residues.

RNase H Cleavage and Kinetics. RNase H kinetics data were obtained using Perkin Elmer UV/VIS spectrophotometer Lambda 40 at 260 nm and 20° C. DNA-conjugates (1.3 nmol) were mixed with the 10-mer RNA **29** (1.3 nmol) in 1.3 ml of buffer C {20 mM Tris·HCl (pH 7.5), 10 mM $MgCl_2$, 100 mM KCl, 2% glycerol and 0.1 mM DTT}. The mixture was heated and equilibrated as done for other physico-chemical measurements and then the absorbance was recorded. Five units of RNase H (Pharmacia Biotech) were added and the solution was incubated at 20° C for 10h, and A_{260} versus time was recorded. From the curve obtained, $t_{0.5}$ (half-life: time at which 50% absorbance change was observed) and $t_{0.99}$ (lifetime of completion: time after which no absorbance change was observed) were calculated.

For studying the inhibition of RNase H mediated cleavage of DNA-conjugates RNA duplexes, by DNA-conjugates DNA duplexes, DNA-conjugates (1μM) were mixed with the 10-mer RNA **29** (1μM) in 600 μl of buffer C and with 10-mer DNA **30** (1μM) in 700 μl of buffer C. After equilibrating the solutions overnight at 4° C, we added five units of RNase H to the solution with the DNA-DNA duplex (700 μl) and incubated it at 20° C for 10 min. Then the solution with the DNA-RNA duplex (600 μl) was added with stirring to allow proper mixing. The resulting solution was incubated at 20° C for 10h, and A_{260} versus time was recorded. From the curve obtained, $t_{0.5}$, $t_{0.99}$ and % $(\text{cleavage})_{\text{inhibition}}$ (TABLE 4) were calculated.

ACKNOWLEDGEMENTS

We thank Swedish Natural Science Research Council (NFR), Swedish Board for Technical Development (NUTEK) and Swedish Engineering Research Council (TFR) for generous financial support. We also thank the Wallenbergstiftelsen, Forskningsrådsnämnden, and University of Uppsala for funds for the purchase of 600 and 500 MHz Bruker DRX NMR spectrometers.

REFERENCES

(1) Belikova, A. M.; Zarytova, V. F.; Grineva, N. I. *Tetrahedron Lett.* **1967**, *37*, 3557-3562.

(2) (a) Letsinger, R. L.; Schott, M. E. *J. Am. Chem. Soc.* **1981**, *103*, 7394-7396. (b) Asseline, U.; Delarue, M.; Lancelot, G.; Toulme, F.; Thuong, N. T.; Montenay-Garestier, T.; Hélène, C. *Proc. Natl. Acad. Sci. USA* **1984**, *81*, 3297-3301.

(3) Reviews: (a) Knorre, D. G.; Vlassov, V. V.; Zarytova, V. F.; Lebedev, A. V.; Federova, O. S. *Design and targeted reactions of oligonucleotide derivatives*; CRC Press: **1994**. (b)Asseline, U.; Thuong, N. T.; Hélène, C. *New J. Chem* **1997**, *21*, 5-17. Recent work: (c)

(4) Reviews: (a) Mesmaeker, A. D.; Häner, R.; Martin, P.; Moser, H. E. *Acc. Chem. Res.* **1995**, *28*, 366-374. (b) Uhlmann, E.; Peymen, A. *Chem. Rev.* **1990**, *90*, 543-584. Recent work: (c) Silver, G.C.; Sun, J-S.; Nguyen, C.H.; Boutorine, A.S.; Bisagni, E.; Hélène, C. *J. Am. Chem. Soc.* **1997**, *119,* 263-268.

(5) Habus, I.; Zhao, Q.; Agrawal, S. *Bioconjugate Chem.* **1995**, *6*, 327-331.

(6) (a) Letsinger, R. L.; Zhang, G.; Sun, D. K.; Ikeuchi, T.; Sarin, P. S. *Proc. Natl. Acad. Sci. USA* **1989**, *86*, 6553. (b) Gryaznov, S. M.; Lloyd, D. H. *Nucleic Acids Res.* **1993**, *21*, 5909-5915. (c) Manoharan, M.; Tivel, K. L.; Cook, P. D. *Tetrahedron Lett.* **1995**,

36, 3651-3654. (d) Rump, E. T.; de Vrueh, R. L. A.; Sliedregt, L. A. J. M.; Biessen, E. A. L.; van Berkel, T. J. C.; Bijsterbosch, M. K. *Bioconjugate Chem.* **1998**, *9*, 341-349.

(7) (a) Boutorin, A. S.; Vlassov, V. V.; S.A., K.; Kutiavin, I. V.; Podyminogin, M. A. *FEBS Lett.* **1984**, *172*, 43-46. (b) Chen, C.; Sigman, D. S. *Proc. Natl. Acad. Sci. USA* **1986**, *83*, 7147-7151. (c) Doan, T. L.; Perrouault, L.; Hélène, C.; Chassignol, M.; Thuong, N. T. *Biochemistry* **1986**, *25*, 6736-6739. (d) Mestre, B.; Pratviel, G.; Meunier, B. *Bioconjugate Chem.* **1995**, *6*, 466-472.

(8) Armitage, B. *Chem. Rev.* **1998**, *98*, 1171-1200.

(9) Trawick, B. N.; Daniher, A. T.; Bashkin, J. K. *Chem. Rev.* **1998**, *98*, 939-960.

(10) (a) Maltseva, T. V.; Sandström, A.; Ivanova, I.; Sergeyev, D.; Zarytova, V.; Chattopadhyaya, J. *J. Biochem. Biophys. Meth.* **1993**, *26*, 173-236. (b) Maltseva, T. V.; Agback, P.; Repkova, M. N.; Venyaminova, A. G.; Ivanova, E. M.; Sandström, A.; Zarytova, V. F.; Chattopadhyaya, J. *Nucleic Acids Res.* **1994**, *22*, 5590- 5599.

(11) Puri, N.; Zamaratski, E.; Sund, C.; Chattopadhyaya, J. *Tetrahedron* **1997**, *53*, 10409-10432 and references therein.

(12) (a) Rajur, S. B.; Robles, J.; Wiederholt, K.; Kuimelis, R. G.; McLaughlin, L. W. *J. Org. Chem.* **1997**, *62*, 523-529. (b) Robles, J.; McLaughlin, L. W. *J. Am. Chem. Soc.* **1997**, *119*, 6014-6021.

(13) (a) Beaucage, S. L.; Caruthers, M. H. *Tetrahedron Lett.* **1981**, *22*, 1859-1862. (b) Beaucage, S. L.; Iyer, R. P. *Tetrahedron* **1993**, *49*, 1925-1963. (c) Beaucage, S. L.; Iyer, R. P. *Tetrahedron* **1993**, *49*, 6123-6194.

(14) McMinn, D. L.; Greenberg, M. M. *J. Am. Chem. Soc.* **1998**, *120*, 3289-3294.

(15) McBride, L. J.; Caruthers, M. H. *Tetrahedron Lett.* **1983**, *20*, 205-208.

(16) Mann, J. S.; Shibata, Y.; Meehan, T. *Bioconjugate Chem.* **1992**, *3*, 554-558.

(17) Lesnik, E. A.; Freier, S. M. *Biochemistry* **1995**, *34*, 10807-10815.

(18) Hunter, C. A.; Sanders, J. K. M. *J. Am. Chem. Soc.* **1990**, *112*, 5525-5534.

(19) Hunter, C. A. *Angew. Chem. Int. Ed. Engl.* **1993**, *32*, 1584-1586.

(20) Gonzalez, C.; Stec, W.; Reynolds, M. A.; James, T. L. *Biochemistry* **1995**, *34*, 4969-4982.

(21) Pachmann, U.; Rigler, R. *Exptl. Cell Res.* **1972**, *72*, 602-608.

(22) Asseline, U.; Toulme, F.; Thuong, N. T.; Delarue, M.; Montenay-Garestier, T.; Hélène, C. *EMBO J.* **1984**, *3*, 795-799.

(23) (a) Sun, J.-S.; Francois, J.-C.; Montenay-Garestier, T.; Saison-Behmoaras, T.; Roig, V.; Thuong, N. T.; Hélène, C. *Proc. Natl. Acad. Sci. USA* **1989**, *86*, 9198-9202. (b) Sun, J.-S.; Asseline, U.; Rouzaud, D.; Montenay-Garestier, T.; Thuong, N. T.; Hélène, C. *Nucleic Acids Res.* **1987**, *15*, 6149-6158.

(24) (a) Kopka, M.; Yoon, C.; Goodsell, D.; Pjura, P.; Dickerson, R. E. *J. Mol. Biol.* **1985**, *183*, 55-61. (b) Coll, M.; Frederick, C. A.; Wang, A. H.-J. *Proc. Natl. Acad. Sci. USA* **1987**, *84*, 8385-8389. (c) Larsen, T. A.; Goodsell, D. S.; Cascia, D.; Grzeskowiak, K.; Dickerson, R. W. *J. Biomol. Stereodyn.* **1989**, *7*, 477-491. (d) Pjura, P.; Grzeskowiak, K.; Dickerson, R. E. *J. Mol. Biol.* **1987**, *197*, 257-271. (e) Teng, M. K.; Usman, N.; Frederick, C. A.; Wang, A. H. *Nucleic Acids Res.* **1988**, *16*, 2671-90. (f) Searle, M. S.; Embrey, K. J. *Nucleic Acids Res.* **1990**, *18*, 3753-62. (g) Fede, A.; Billeter, M.; Leupin, W.; Wuthrich, K. *Structure* **1993**, *1*, 177-186.

(25) Kumar, S.; Reed, M. W.; Gamper, Jr, H. B.; Gorn, V. V.; Lukhtanov, E. A.; Foti, M.; West, M.; Meyer, Jr, R. B.; Schweitzer, B. I. *Nucleic Acids Res.* **1998**, *26*, 831-838.

(26) Zimmer, C.; Wähnert, U. *Prog. Biophys. Mol. Biol.* **1986**, *47*, 31-112.

(27) Lootiens, F. G.; Regenfuss, P.; Zechel, A.; Dumortier, L.; Clegg, R. M. *Biochemistry* **1990**, *29*, 9029-9039.

(28) Davis, T. M.; McFail-Isom, L.; Keane, E.; Williams, L. D. *Biochemistry* **1998**, *37*,

6975- 6978.
(29) Hung, S.-H.; Yu, Q.; Gray, D. M.; Ratliff, R. L. *Nucleic Acids Res.* **1994**, *22*, 4326-4334.
(30) Allen, F. S.; Gray, D. M.; Roberts, G. P.; Tinoco, I., Jr *Biopolymers* **1972**, *11*, 853-879.
(31) (a) Maltseva, T. V.; Agback, P.; Chattopadhyaya, J. *Nucleic Acids Res.* **1993**, *21*, 4206-4252. (b) Maltseva, T. V.; Chattopadhyaya, J. *Tetrahedron* **1995**, *51*, 5501-5508. (c) Maltseva, T. V.; Zarytova, V. F.; Chattopadhyaya, J. *J. Biochem. Biophys. Meth.* **1995**, *30*, 163-177.
(32) Clark, C. L.; Cecil, P. K.; Singh, D.; Gray, D. M. *Nucleic Acids Res.* **1997**, *25*, 4098-4105.
(33) Newcomb, L. F.; Gellman, S. H. *J. Am. Chem. Soc.* **1994**, *116*, 4993-4994.
(34) Vesnaver, G.; Breslauer, K. J. *Proc. Natl. Acad. Sci. USA* **1991**, *88*, 3569-3573.
(35) Searle, M. S.; Williams, D. H. *Nucleic Acids Res.* **1993**, *21*, 2051-2056.
(36) Stein, C. A.; Subasinghe, C.; Shinozuka, K.; Cohen, J. S. *Nucl. Acids Res.* **1988**, *16*, 3209-3221.
(37) Knudsen, H.; Nielsen, P. E. *Nucleic Acids Res.* **1996**, *20*, 494-500.
(38) Cedergren, R.; Grosjean, H. *Biochem. Cell Biol.* **1987**, *65*, 677-692.
(39) Donis-Keller, H. *Nucleic Acids Res.* **1979**, *7*, 179-192.
(40) Schatz, O.; Mous, J.; Le Grice, S. F. J. *EMBO J.* **1990**, *9*, 1171-1176.
(41) Agrawal, S.; Mayrand, S. H.; Zamecnik, P. C.; Pederson, T. *Proc. Natl. Acad. Sci. USA* **1990**, *87*, 1401-1405.
(42) Agrawal, S.; Jiang, Z.; Zhao, Q.; Shaw, D.; Cai, Q.; Roskey, A.; Channavajjala, L.; Saxinger, C.; Zhang, R. *Proc. Natl. Acad. Sci. USA* **1997**, *94*, 2620-2625.
(43) The RNase H cleavages were monitored at 20° C, and the % duplex state for each pair of DNA-conjugate and RNA were as follows: **14•29** (80%), **17•29** (88%), **19•29** (74%), **21•29** (87%), **23•29** (80%) & **27•29** (65%). These show that the population of the DNA-conjugates + target **29** in duplex state were in the 0.85 - 1.14 nmol range at the initiation of the study. Thus the concentration of the DNA-RNA duplex was greater than the substrate requirement of RNase H [0.25 nmol; one Unit of RNase H (*E. coli*) digests 0.05 nmol of DNA-RNA heteroduplex in 1 min at 37° C]. Hence the rates of cleavage of the heteroduplexes by RNase H are comparable, but only in a qualitative manner. Once the exision of the RNA strand by RNase H commences it is difficult to estimate the population of the duplex state for each ssDNA-conjugate, since they all have different relative cleavage rates. Ideally, one should perform the cleavage study under a condition when DNA-RNA duplex population is >99%, which is at ~10° C for our duplexes. However monitoring of the RNase H cleavage of DNA-RNA duplex at that low temperature is far from quasiphysiological condition.
(44) Gutierrez, A. J.; Matteucci, M. D.; Grant, D.; Matsumura, S.; Wagner, R. W.; Froehler, B. C. *Biochemistry* **1997**, *36*, 743-748 and references therein.
(45) Damha, M. J.; Wilds, C. J.; Noronha, A.; Brukner, I.; Borkow, G.; Arion, D.; Parniak, M. A. *J. Am. Chem. Soc.* **1998**, *120*, 12976-12977.
(46) Kool, E. T. *Chem. Rev.* **1997**, *97*, 1473-1487.
(47) Matray, T. J.; Kool, E. T. *J. Am. Chem. Soc.* **1998**, *120*, 6191-6192.
(48) Zamaratski, E.; Chattopadhyaya, J. *Tetrahedron* **1998**, *54*, 8183-8206.
(49) Fasman, G. *In Handbook of Biochemistry and Molecular Biology, Vol. I*; CRC Press: Ohio. **1975**, pp 589.